(Received 7 January 2026, Accepted 4 February 2026, Scheduled 13 March 2026)

Intelligent Harmonic Current Suppression Algorithm for Permanent Magnet Synchronous Motors in Industrial Servo Systems

Xing Zhang[1,*], Lin Wang[2], Lihui Guo[1], Guanghui Zhu[1], Shibo Jin[1], and Yanyan Ye[3]

[1]*School of Electrical Engineering, Xuchang University, Xuchang 461000, China*
[2]*Jiangsu Changjiang Intelligent Manufacturing Research Institute Co., Ltd., Changzhou 213001, China*
[3]*Xuchang Power Supply Company of State Grid Henan Electric Power Company, Xuchang 461100, China*

ABSTRACT: A dual adaptive neural network-based harmonic compensation algorithm is proposed to improve the low-speed machining accuracy of permanent magnet synchronous motor (PMSM) drives. First, the mechanism of harmonic current generation and its influence on torque ripple and speed fluctuation in PMSMs is analyzed. Second, the structure of the dual adaptive neural network is designed: the first network is used to extract harmonic current components in real time, and the second network dynamically generates corresponding harmonic voltage compensation signals to suppress current distortion, with the advantages of fast dynamic response and high compensation accuracy. Finally, the proposed method is verified on an experimental platform. The experimental results show that the 6th harmonic amplitude is suppressed from 0.094 to 0.016, and the 12th harmonic amplitude is reduced from 0.025 to 0.004, which is significantly better than the traditional compensation method. The proposed algorithm effectively reduces torque ripple and speed fluctuations, thereby improving the control accuracy and machining performance of the PMSM drive system.

1. INTRODUCTION

In the field of computer numerical control (CNC) machine tools, permanent magnet synchronous motor (PMSM) spindles have received widespread attention because of their high efficiency and precise controllability. Compared to induction motor spindles, they have lower heat generation, more stable operation, higher power density, and more compact structure [1, 2].

To maintain the high machining accuracy of CNC grinders, it is necessary to suppress all factors that may compromise accuracy, primarily including mechanical and electrical control. Firstly, the core reasons for the decrease in machining accuracy in mechanical aspects mainly include rotational errors, thermal deformation, stress deformation, vibration, bearing degradation, clamping errors, etc. In terms of electrical control, there are mainly thermal deformation compensation, servo loop optimization, vibration suppression control, resonance avoidance, and intelligent parameter adjustment. Among them, vibration control is an essential part of the control process of CNC grinding machines. Harmonic current is the main factor causing vibration of the electric spindle; therefore, it is imperative to develop an efficient harmonic current suppression strategy [3–5].

At present, the research on suppressing stator current harmonics in PMSM mainly focuses on two technical approaches: one is the optimization design of the motor's electromagnetic structure, and the other is the improvement of system control algorithms. In terms of motor design, the mainstream method involves evaluating the electromagnetic structure through finite element method (FEM) and adjusting the stator rotor structure and winding layout accordingly to improve the sinuosity of the back electromotive force (EMF), thereby reducing the inherent harmonic components of the motor itself [6]. In terms of control algorithms, the main focus is on analyzing harmonic components and compensating control based on the different harmonics.

In the existing research on stator current harmonic suppression of PMSM, the main focus is on compensating for harmonic currents caused by nonlinear and non-sinusoidal inverter electromotive forces. In [7], a random asymmetric space vector pulse width modulation (SVPWM) based on Markov chains is used to suppress high-order inverter harmonics in outer loop control. However, the problem of low-order harmonic components in this method has not been solved under low-inductance operating conditions. Dai et al. [8] proposed the Adaptive Harmonic Reference Correcting Current Injection (AHRCC) method for harmonic suppression, which effectively eliminates low-order current harmonics caused by nonlinear and non-sinusoidal inverter electromotive forces, while reducing motor torque ripple and losses. In [9], by reconstructing frequency control and decoupling DC link voltage, the compensation link is extended to the grid side, effectively suppressing harmonic currents. In [10], multiple reference frames are introduced in the low-speed range to extract speed harmonics and suppress harmonic currents. However, it incurs computational overhead related to fundamental wave reconstruction, requiring processors with strong computing power to partici-

* Corresponding author: Xing Zhang (zhangxing03230@163.com).

pate in the operation. In [11], the use of synthetic prediction models and deadbeat predictive control with integral compensation reduced steady-state errors at low switching frequencies and achieved suppression of harmonic currents. A virtual even order fractional order repetitive control and harmonic control strategy is constructed in [12, 13], and precise harmonic suppression is achieved. In [14], harmonics are further treated as concentrated disturbances, and unified observations are made using a multi-harmonic inversion extended state observer and an improved Active Disturbance Rejection Control (ADRC). In [15], ADRC is integrated with a dedicated harmonic algorithm to balance accuracy and robustness. In addition, [16] provides a stability compensation method for all the above control structures through small signal modeling.

In summary, the above control algorithms typically have inherent limitations, including strong scene dependence, significant trade-offs between high-precision observation and real-time computational performance, and a lack of collaborative optimization among multiple suppression methods. To address these issues, this paper proposes an adaptive harmonic current suppression algorithm based on neural networks. In this algorithm, the 5th and 7th harmonic components in the three-phase current are first obtained through the first adaptive neural network algorithm, and then the compensation voltage is calculated through the second adaptive neural network algorithm. Through the high-performance control mechanism of this algorithm, the problem of harmonic current is effectively solved in real time, and it exhibits excellent adaptability to complex operating conditions. The experimental results show that the algorithm significantly improves the harmonic current suppression performance during the low-speed operation of the motor, thereby effectively improving the machining accuracy of the CNC grinder.

2. MATHEMATICAL MODEL AND MECHANISM OF HARMONIC GENERATION

The connection modes of the three-phase stator windings of a PMSM include delta- and Y-shaped connections. Under ideal symmetrical winding conditions, the Y-shaped connection used in this study exhibits half-wave symmetry of the back electromagnetic field (EMF) waveform. This symmetry determines that there are no even-order harmonic components in the waveform, and the phase difference of the three-phase n-th order harmonic current remains constant at $2n\pi/3$. Thus, the stator harmonic current can be expressed as:

$$\begin{cases} I_{an} = I_n \cos\left(n\omega_e t + \theta_{n0}\right) \\ I_{bn} = I_n \cos\left(n\omega_e t - \dfrac{2}{3}n\pi + \theta_{n0}\right) \\ I_{cn} = I_n \cos\left(n\omega_e t + \dfrac{2}{3}n\pi + \theta_{n0}\right) \end{cases} \tag{1}$$

where I_{an}, I_{bn}, and I_{cn} are the three-phase n-th harmonic currents of a, b, and c, respectively; I_n is the amplitude of the n-th harmonic current; θ_{n0} is the initial phase of the n-th harmonic current; ω_e is the electrical angular velocity of the motor; ω_e is the electrical angular velocity of the motor. For harmonic order $n = 3k$ (where $k \in \mathbb{N}^+$), the n-th harmonic components of the three-phase currents have equal amplitudes and the same phase. However, stator windings with a Y-shaped connection cannot provide a closed path for the $3k$-th harmonic currents, so such harmonic components do not actually exist in the windings.

When the harmonic order satisfies $n = 6k + 1$ ($k \in \mathbb{N}^+$):

$$\begin{cases} i_a^{(n)} \text{ leads } i_b^{(n)} \text{ by an angle of } 2n\pi/3 \\ i_a^{(n)} \text{ lags } i_c^{(n)} \text{ by an angle of } 2n\pi/3 \end{cases} \tag{2}$$

This phase sequence relationship is consistent with that of the fundamental current.

When the harmonic order satisfies $n = 6k - 1$ ($k \in \mathbb{N}^+$):

$$\begin{cases} i_a^{(n)} \text{ lags } i_b^{(n)} \text{ by an angle of } 2n\pi/3 \\ i_a^{(n)} \text{ leads } i_c^{(n)} \text{ by an angle of } 2n\pi/3 \end{cases} \tag{3}$$

This phase sequence relationship is opposite to that of the fundamental current.

Based on the above harmonic constraint characteristics, the complete expression of the three-phase currents (i_a, i_b, i_c) of the PMSM can be expressed as [15]:

$$\begin{cases} i_a = I_1 \cos(\omega_e t + \theta_1) + I_5 \cos\left(5\omega_e t + \theta_5\right) + \\ \quad I_7 \cos\left(7\omega_e t + \theta_7\right) + \ldots \\ i_b = I_1 \cos\left(\omega_e t - \dfrac{2}{3}\pi + \theta_1\right) + I_5 \cos\left(5\omega_e t + \dfrac{2}{3}\pi + \theta_5\right) + \\ \quad I_7 \cos\left(7\omega_e t - \dfrac{2}{3}\pi + \theta_7\right) + \ldots \\ i_c = I_1 \cos\left(\omega_e t + \dfrac{2}{3}\pi + \theta_1\right) + I_5 \cos\left(5\omega_e t - \dfrac{2}{3}\pi + \theta_5\right) + \\ \quad I_7 \cos\left(7\omega_e t + \dfrac{2}{3}\pi + \theta_7\right) + \ldots \end{cases} \tag{4}$$

$$T_{abc}^{dq} = \frac{2}{3}\begin{bmatrix} \cos\left(\omega_e t\right) & \cos\left(\omega_e t - \dfrac{2\pi}{3}\right) & \cos\left(\omega_e t + \dfrac{2\pi}{3}\right) \\ -\sin\left(\omega_e t\right) & -\sin\left(\omega_e t - \dfrac{2\pi}{3}\right) & -\sin\left(\omega_e t + \dfrac{2\pi}{3}\right) \end{bmatrix} \tag{5}$$

After the transformation shown in (5), the current expression in the two-phase rotating coordinate system can be obtained by using (4) [15]:

$$\begin{cases} i_d = I_1 \cos\theta_1 + I_5 \cos\left(-6\omega_e t + \theta_5\right) + \\ \quad I_7 \cos\left(6\omega_e t + \theta_7\right) + \ldots \\ i_q = I_1 \sin\theta_1 + I_5 \sin\left(-6\omega_e t + \theta_5\right) + \\ \quad I_7 \sin\left(6\omega_e t + \theta_7\right) + \ldots \end{cases} \tag{6}$$

where i_d and i_q are the stator currents in the d- and q-axis rotating coordinate systems, respectively.

Based on the mathematical description in Eqs. (4) and (6), when the fundamental angular velocity is adopted as the reference velocity of the synchronous rotating coordinate system, the DC components are presented by the fundamental components in the d-axis and q-axis currents through the Park transformation defined by Eq. (5). Based on this transformation principle, specific harmonic components in the extended d-q axis system can be decoupled and extracted by constructing multiple synchronous reference frames (MSRFs).

We define the coordinate transformation matrix from the fundamental synchronous rotating coordinate system to the 5th harmonic synchronous rotating coordinate system as:

$$T_{dq}^{dq5} = \begin{bmatrix} \cos(-6\omega_e t) & \sin(-6\omega_e t) \\ -\sin(-6\omega_e t) & \cos(-6\omega_e t) \end{bmatrix} \tag{7}$$

The transformation matrix for converting the abc coordinate system to a 5th synchronous rotation coordinate system is:

$$\begin{aligned} T_{abc}^{dq5} &= T_{dq}^{dq5} T_{abc}^{dq} \\ &= \frac{2}{3}\begin{bmatrix} \cos(-5\omega_e t) & \cos\left(5\omega_e t + \frac{2\pi}{3}\right) & \cos\left(5\omega_e t - \frac{2\pi}{3}\right) \\ \sin(-5\omega_e t) & \sin\left(5\omega_e t + \frac{2\pi}{3}\right) & -\sin\left(5\omega_e t - \frac{2\pi}{3}\right) \end{bmatrix} \end{aligned} \tag{8}$$

By mapping Eq. (4), using the coordinate transformation matrix defined in Eq. (8), the analytical expression of the motor stator currents in the 5th harmonic synchronous rotating coordinate system (the d_5-q_5 axis system) can be expressed as

$$\begin{cases} i_{d5} = I_1 \cos(6\omega_e t + \theta_1) + I_5 \cos\theta_5 + I_7 \cos(12\omega_e t + \theta_7) \\ i_{q5} = I_1 \sin(6\omega_e t + \theta_1) + I_5 \sin\theta_5 + I_7 \sin(12\omega_e t + \theta_7) \end{cases} \tag{9}$$

where i_{d5} and i_{q5} are the d- and q-axis components of the stator current in the 5th synchronous rotating coordinate system, respectively.

Similarly, the expression of the stator current in the 7th synchronous rotating coordinate system is

$$\begin{cases} i_{d7} = I_1 \cos(6\omega_e t - \theta_1) + I_5 \cos(12\omega_e t - \theta_5) + I_7 \cos\theta_7 \\ i_{q7} = -I_1 \sin(6\omega_e t - \theta_1) - I_5 \sin(12\omega_e t - \theta_5) + I_7 \sin\theta_7 \end{cases} \tag{10}$$

where i_{d7} and i_{q7} are the d- and q-axis components of the stator current in the 7th synchronous rotating coordinate system, respectively.

3. HARMONIC CURRENT SUPPRESSION METHOD

3.1. Traditional Method

Key conclusions can be derived from the mathematical characterizations of Eqs. (8) and (9): In the 5th and 7th harmonic synchronous rotating coordinate systems (d_5-q_5 axis system and d_7-q_7 axis system), the harmonic components of the corresponding orders (i.e., the 5th and 7th harmonics) are all mapped to DC components, whereas the fundamental component and other integer-order harmonics appear as AC components. This frequency-domain decoupling characteristic provides a theoretical basis for the separation and extraction of harmonic currents. The structure of the traditional harmonic current extraction system constructed based on it is shown in Fig. 1, where θ_e is the rotor position angle of the motor; i_{d5h} and i_{q5h} represent the direct-axis and quadrature-axis components of the 5th harmonic current in the d_5-q_5 coordinate system, respectively; and i_{d7h} and i_{q7h} represent the direct-axis and quadrature-axis components of the 7th harmonic current in the d_7-q_7 coordinate system, respectively.

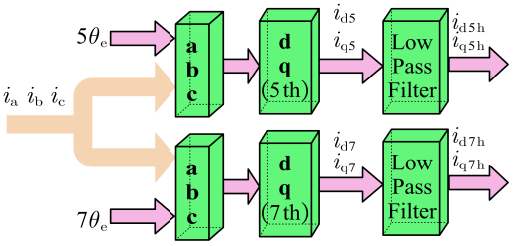

FIGURE 1. Structure of traditional harmonic current extraction system based on multiple synchronous rotating frames.

The 5th and 7th harmonic current components processed by the closed-loop harmonic current extraction module are mathematically characterized in their respective synchronous rotating coordinate systems as follows:

$$\begin{cases} i_{\mathrm{d5(7)h}} = \mathrm{LPF}\left(i_{\mathrm{d5(7)}}\right) = I_{5(7)} \cos\theta_{5(7)} \\ i_{\mathrm{q5(7)h}} = \mathrm{LPF}\left(i_{\mathrm{q5(7)}}\right) = I_{5(7)} \sin\theta_{5(7)} \end{cases} \tag{11}$$

In the harmonic current extraction architecture based on multiple synchronous rotating coordinate systems (the 5th/7th d-q axis systems), low-pass filters (LPFs) are typically employed to separate the DC components of the target harmonics. However, the dynamic characteristics of the LPFs can be equivalent to first-order (or higher-order) inertial elements [16]:

$$G_{\mathrm{LPF}}(s) = \frac{1}{1+\tau s} \quad \text{or} \quad \frac{1}{(1+\tau s)^n} \quad (n \geq 2) \tag{12}$$

where τ is the time constant, and its physical nature introduces a non-negligible phase lag [17].

$$\phi_{\mathrm{lag}} = -\arctan(\omega\tau) \quad \text{(first-order system)} \tag{13}$$

In the traditional harmonic current suppression strategy, as shown in the control architecture in Fig. 2, the extracted 5th and 7th harmonic current components, i_{d5h}, i_{q5h}, i_{d7h}, and i_{q7h}, serve as feedback inputs and form error signals with their respective reference values, $i_{\mathrm{dq5h\_ref}}$ and $i_{\mathrm{dq7h\_ref}}$. These errors are processed by a proportional-integral (PI) controller to generate the corresponding harmonic compensation voltage commands.

In this control architecture, the introduction of multiple PI controllers imposes dual bottlenecks. First, the inherent computational delay of the control loop causes a phase deviation in the harmonic compensation voltage, which significantly impairs the suppression effectiveness of harmonic currents. Second, the coordinated tuning of multiple sets of PI parameters significantly increases the complexity of algorithm implementation.

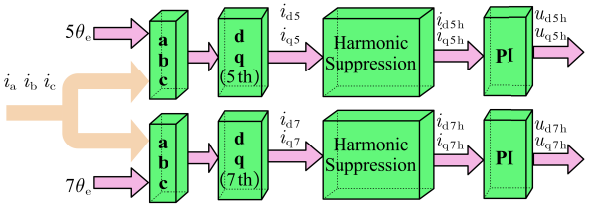

FIGURE 2. Traditional harmonic current suppression strategy based on multi-PI controllers.

3.2. The Proposed Harmonic Current Suppression Algorithm

The multi-PI controller-based harmonic current suppression algorithm used in the above figure can effectively suppress the DC components. However, the PI controller exhibited poor suppression performance for high-frequency harmonic components. Thus, a multi-network learning-based harmonic current suppression algorithm was proposed. A schematic block diagram of this algorithm is shown in Fig. 3, where the first learning network is used to extract harmonic currents. Its calculation process is as follows:

$$\begin{cases} \hat{i}_{\mathrm{d5}} = i_{\mathrm{d50}} + i_{\mathrm{d5h}} = \omega_{\mathrm{d50}} + \omega_{\mathrm{d5a}}\cos(6\theta_{\mathrm{e}}) + \omega_{\mathrm{d5b}}\sin(6\theta_{\mathrm{e}}) + \\ \quad \omega_{\mathrm{d7a}}\cos(12\theta_{\mathrm{e}}) + \omega_{\mathrm{d7b}}\sin(12\theta_{\mathrm{e}}) \\ \hat{i}_{\mathrm{q5}} = i_{\mathrm{q50}} + i_{\mathrm{q5h}} = \omega_{\mathrm{q50}} + \omega_{\mathrm{q5a}}\cos(6\theta_{\mathrm{e}}) + \omega_{\mathrm{q5b}}\sin(6\theta_{\mathrm{e}}) + \\ \quad \omega_{\mathrm{q7a}}\cos(12\theta_{\mathrm{e}}) + \omega_{\mathrm{q7b}}\sin(12\theta_{\mathrm{e}}) \end{cases} \tag{14}$$

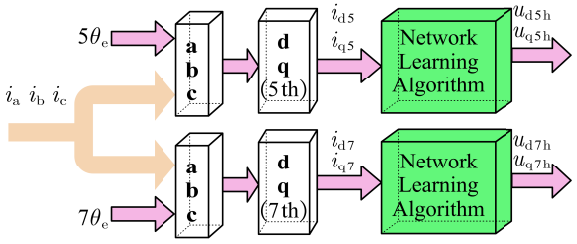

FIGURE 3. Schematic diagram of multi-network learning-based harmonic current suppression algorithm.

The calculation of the weight update network is mainly derived from the error function, which is defined as follows [8]:

$$E = \frac{1}{2}(d - O)^2 \tag{15}$$

By differentiating the error function using the gradient descent method, the weight calculation process can be obtained as follows:

$$\Delta\boldsymbol{\omega} = \eta\,(\boldsymbol{d} - \boldsymbol{O}) \cdot \boldsymbol{O}_{\mathrm{i}} \tag{16}$$

where $\Delta\boldsymbol{\omega}$ is the weight change; η is the learning rate; $\boldsymbol{d}$ is the target value; $\boldsymbol{O}$ is the output value of the adaptive neural network; $\boldsymbol{O}_{\mathrm{i}}$ is the input variable.

After passing through the first adaptive network controller shown in Fig. 4, the corresponding harmonic current values can be obtained. Subsequently, a second adaptive network controller was designed to calculate the corresponding voltage

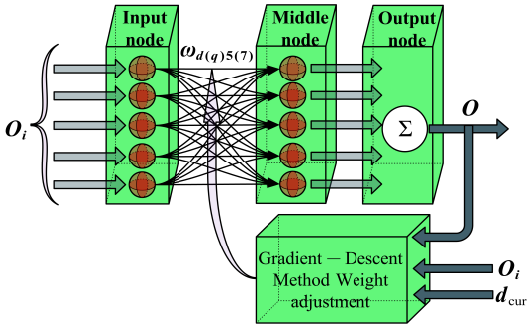

FIGURE 4. Principle block diagram of the first adaptive network controller.

compensation values, and its calculation process is as follows:

$$\begin{cases} u_{\mathrm{d5(7)h}} = \nu_{\mathrm{d5a}}\cos(6\theta_{\mathrm{e}}) + \nu_{\mathrm{d5b}}\sin(6\theta_{\mathrm{e}}) + \\ \quad \nu_{\mathrm{d7a}}\cos(12\theta_{\mathrm{e}}) + \nu_{\mathrm{d7b}}\sin(12\theta_{\mathrm{e}}) \\ u_{\mathrm{q5(7)h}} = \nu_{\mathrm{q5a}}\cos(6\theta_{\mathrm{e}}) + \nu_{\mathrm{q5b}}\sin(6\theta_{\mathrm{e}}) + \\ \quad \nu_{\mathrm{q7a}}\cos(12\theta_{\mathrm{e}}) + \nu_{\mathrm{q7b}}\sin(12\theta_{\mathrm{e}}) \end{cases} \tag{17}$$

Similar to the first adaptive network controller, the weight update process of the second adaptive network controller is as follows:

$$\begin{cases} \boldsymbol{\nu}_{\mathrm{d5(7)}}(k+1) = \boldsymbol{\nu}_{\mathrm{d5(7)}}(k) + 2\eta_2 \boldsymbol{e}_{\mathrm{d5(7)}}(k)\boldsymbol{r}_2(k) \\ \boldsymbol{\nu}_{\mathrm{q5(7)}}(k+1) = \boldsymbol{\nu}_{\mathrm{q5(7)}}(k) + 2\eta_2 \boldsymbol{e}_{\mathrm{q5(7)}}(k)\boldsymbol{r}_2(k) \end{cases} \tag{18}$$

where $\boldsymbol{r}_2(k) = \left[\cos(6\theta_{\mathrm{e}}) \quad \sin(6\theta_{\mathrm{e}}) \quad \cos(12\theta_{\mathrm{e}}) \quad \sin(6\theta_{\mathrm{e}})\right]^{\mathrm{T}}$, η_2 is the learning rate, and $\boldsymbol{e}_{\mathrm{dq5(7)}}$ are the error terms.

A schematic of the controller corresponding to the expression of the second adaptive network controller is shown in Fig. 5.

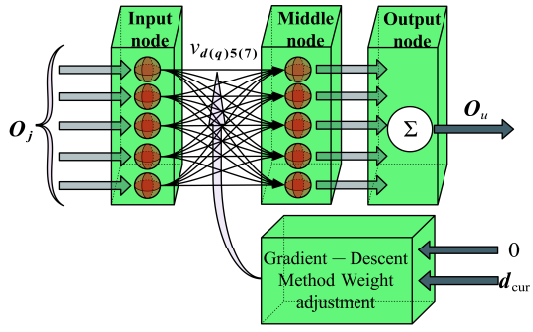

FIGURE 5. Principle block diagram of the second adaptive network controller.

The above method is applicable not only to suppressing the 5th and 7th harmonics but also to suppressing harmonic currents of other orders. The overall control block diagram of the harmonic current suppression method based on a dual-adaptive network controller is shown in Fig. 6. The three-phase ABC current is collected by the current sensor, and after the harmonic current compensation algorithm, the required compensation voltage $u_{\mathrm{d(q)5h}}$ was obtained. After obtaining the compensation voltage, inject it into the forward channel and add it

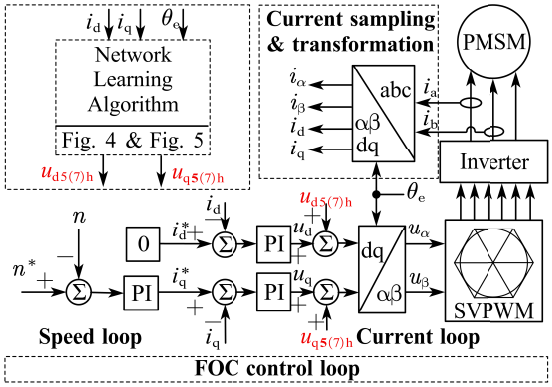

FIGURE 6. Overall control block diagram of dual adaptive network-based harmonic current suppression method.

to the $u_{d(q)}$ voltage. By actively injecting harmonic compensation signals, the suppression function of harmonic signals in the forward channel is achieved, effectively suppressing harmonic currents.

4. EXPERIMENTAL VERIFICATION

To verify the effectiveness of the proposed algorithm, it was tested on the experimental platform shown in Fig. 7. The primary parameters of the experimental prototype are listed in Table 1. The core control unit of the experimental platform is TMS320F28335 produced by TI company, and the Power Drive module is PS21965 Intelligent Power Module produced by Mitsubishi Company. The number of addition and subtraction is 20; the number of multiplication and division is 24; and the number of sine and cosine is 16. The amount of calculation meets the real-time requirements. During the experiment, the starting speed of the prototype is set to 100 r/min. At 0.5 s, a sudden load of 0.1 N·m is applied. At 1 s, the speed is suddenly changed to 200 r/min, and at 1.5 s, a sudden load of 0.2 N·m is applied.

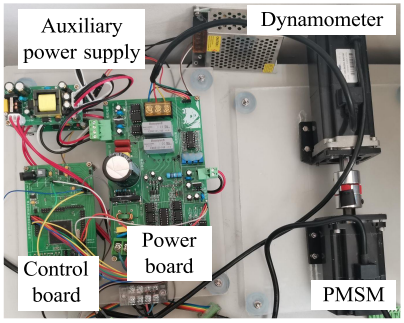

FIGURE 7. Experimental platform for PMSM harmonic current suppression test.

Figure 8 shows the vector PI control method without compensation. Under uncompensated conditions, the speed and current waveforms of the PMSM drive system exhibit significant degradation characteristics. The speed waveform exhibits severe fluctuations at various operating stages, with amplitudes as high as 65 r/min, 83 r/min, 100 r/min, and 105 r/min, respectively. There are obvious high-frequency jitter and instantaneous spikes in the waveform, especially in the low-speed range, showing severe instability. At the same time, the current waveform distortion is severe, and the direct axis current i_d exhibits significant high-frequency oscillations, while the ripple amplitude of the cross-axis current i_q reaches 0.28 A, with high harmonic content. It indicates that without harmonic suppression measures, the harmonic current output by the inverter is directly converted into significant torque ripple, leading to speed fluctuations, and the control accuracy and dynamic performance of the system are at the worst level.

TABLE 1. Parameters of the Test PMSM.

Parameter	Value
Resistance R_s	1.1 Ω
Inductance L_s	5.8 mH
Flux Linkage λ	0.16 Wb
Voltage U	36 V
Current I	4.2 A
Electromagnetic Torque T_e	2.2 Nm
Pole Pairs	50

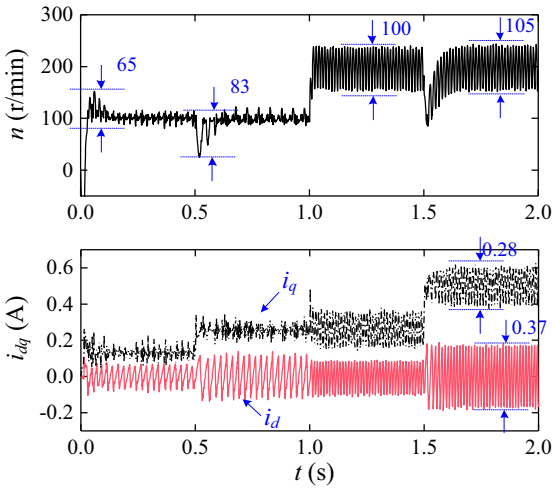

FIGURE 8. Waveforms of rotational speed and dq-axis currents under PI control method.

Figure 9 shows the speed and current waveforms after traditional compensation methods. It can be seen from Fig. 9 that the system performance has been improved to a certain extent. The amplitude of the speed fluctuation is effectively suppressed, dropping to 50 r/min, 23 r/min, and 49 r/min, respectively. The smoothness of the waveform was improved, and the amplitude of the instantaneous peak is significantly reduced. The quality of the current waveform has also been improved, with a reduction in the oscillation amplitude of the direct axis current i_d and a decrease in the ripple amplitude of the quadrature axis current i_q to 0.25 A. It indicates that traditional compensation strategies have, to some extent, suppressed harmonic currents, weakened the impact of torque ripple on speed, and improved system stability. However, significant current distortion and speed fluctuations can still be observed from the waveform, in-

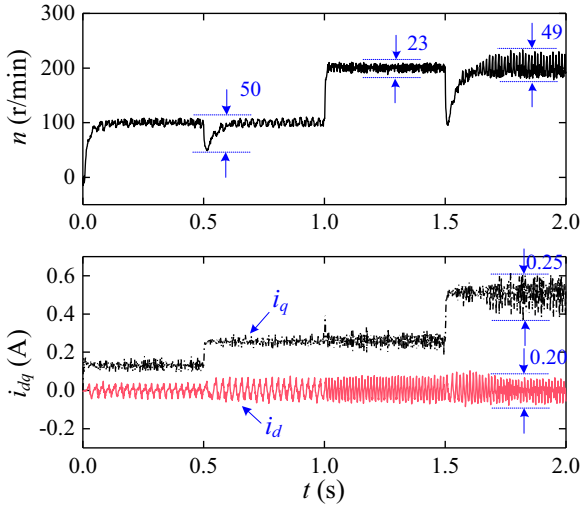

FIGURE 9. Waveforms of rotational speed and dq-axis currents under traditional control method.

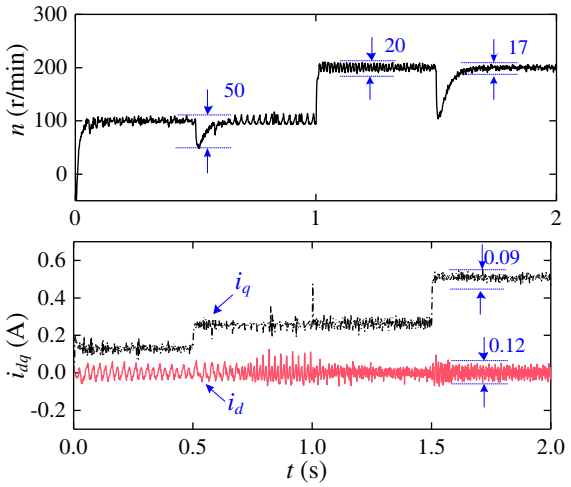

FIGURE 10. Waveforms of rotational speed and dq-axis currents under the proposed control method.

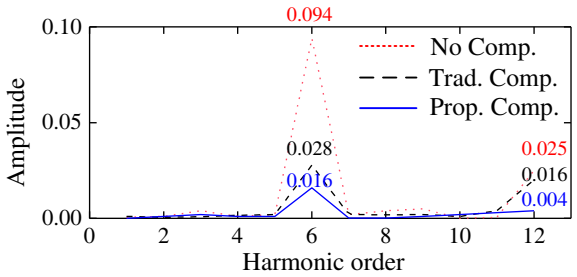

FIGURE 11. Fourier spectrum analysis of q-axis harmonic current.

dicating a limited ability to suppress high-order harmonics and a bottleneck in performance improvement.

The speed and current waveforms of the proposed method are shown in Fig. 10. Under the proposed compensation method, the control performance of the system has been significantly optimized. The speed fluctuation is significantly reduced, with fluctuation amplitudes of only 50 r/min, 20 r/min, and 17 r/min in each stage. The waveform is the smoothest, with almost no obvious instantaneous peaks, and exhibits excellent stability in both low-speed and dynamic response processes. The quality of the current waveform reaches its optimal level, with a significant reduction in the oscillation amplitude of the direct axis current i_d and a ripple amplitude of 0.12 A. The ripple amplitude of the quadrature axis current i_q is further reduced to 0.09 A, effectively suppressing harmonic currents and significantly improving current tracking accuracy. It fully validates the effectiveness and superiority of the proposed method in suppressing harmonic currents, reducing torque ripple, and improving system steady-state accuracy and dynamic performance, and its control effect is comprehensively superior to traditional compensation methods.

Figure 11 shows the harmonic spectrum analysis of the q-axis current signal under three control strategies, which clearly displays the amplitude distribution of each harmonic. From the spectral characteristics, the current harmonics under the three operating conditions are mainly concentrated in the 6th and 12th orders, which is completely consistent with the theoretical analysis of the synthesis of the 6th and 12th harmonics of the current harmonics in the dq coordinate system. Under uncompensated conditions, the amplitude of the 6th harmonic is as high as 0.094, and the amplitude of the 12th harmonic is 0.025, with the highest harmonic content. This is the fundamental reason for the severe torque ripple and speed fluctuation in the system. After using traditional compensation methods, the amplitude of the 6th harmonic decreased to 0.028, and the amplitude of the 12th harmonic decreased to 0.016. The harmonic suppression effect was improved to some extent, but there were still significant residual harmonics, which limited the improvement of system performance. In contrast, the proposed method shows excellent harmonic suppression performance. The 6th harmonic is reduced to 0.016, and the 12th harmonic is reduced to 0.004, effectively eliminating the main harmonic components. The advantages of the proposed method in restraining harmonic currents and reducing torque ripple are proved from the frequency domain level, which is highly consistent with the conclusions of the time-domain waveform analysis, fully verifying the effectiveness and progressiveness of the proposed method.

5. CONCLUSIONS

This article proposes a method based on a dual adaptive neural network algorithm to calculate the harmonic current part that needs to be compensated, in order to improve the machining accuracy of permanent magnet synchronous motors. In the proposed algorithm, the first adaptive neural network is used to obtain harmonic current components and input them into the second adaptive neural network. The second adaptive neural network compensates for harmonic voltages by adjusting weights, which has the advantages of fast dynamic response and high compensation accuracy. The experimental results show that the proposed method significantly improves the harmonic suppression effect: compared with the uncompensated condition, the cross-axis current i_q ripple decreases from 0.28 A to

0.09 A, and the low-speed steady-state speed fluctuation decreases from 105 r/min to 17 r/min. In the frequency domain, the amplitude of the 6th harmonic is suppressed from 0.094 to 0.016, and the amplitude of the 12th harmonic is reduced from 0.025 to 0.004, which is superior to traditional compensation methods. This method effectively reduces torque ripple and speed fluctuation, improving system control accuracy and machining performance.

ACKNOWLEDGEMENT

This work was supported by the Key Technology R&D Program of Henan Province of China (No. 252102240102), the Undergraduate Innovation Training Program (No. 202510480005), the Natural Science Foundation of Henan Province (No. 252300420496), and the Key Scientific Research Project in Universities of Henan Province (No. 25A470011).

REFERENCES

[1] Zhao, H., S. Yu, and F. Sun, "Harmonic suppression and torque ripple reduction of a high-speed permanent magnet spindle motor," *IEEE Access*, Vol. 9, 51 695–51 702, 2021.

[2] Wang, Y., J. Xi, and C. Xie, "Research on flux-weakening control with single current regulator of PMSM based on parameter identification," *IEICE Transactions on Electronics*, Vol. E108.C, No. 8, 402–411, 2025.

[3] Wang, X., Y. Xiang, C. Qu, F. Han, and D. Xu, "Single closed-loop active disturbance rejection control strategy of permanent magnet synchronous motor based on compensation function," *IEICE Electronics Express*, Vol. 21, No. 17, 20240281, 2024.

[4] Yang, H., J.-W. Tang, and Y.-R. Chien, "Application of new sliding mode control in vector control of PMSM," *IEICE Electronics Express*, Vol. 19, No. 13, 20220156, 2022.

[5] Zhang, Y., H. Wu, Y.-R. Chien, and J. Tang, "Vector control of permanent magnet synchronous motor drive system based on new sliding mode control," *IEICE Electronics Express*, Vol. 20, No. 23, 20230263, 2023.

[6] Wu, K., Y. Zhang, W. Lu, Y. Qi, and W. Shi, "Harmonic suppression in permanent magnet synchronous motor currents based on quasi-proportional-resonant sliding mode control," *Applied Sciences*, Vol. 14, No. 16, 7206, 2024.

[7] Yang, Y., W. Song, Y. Ge, and P. Wheeler, "A Markov chain random asymmetrical SVPWM method to suppress high-frequency harmonics of output current in an IMC-PMSM system," *IEEE Transactions on Power Electronics*, Vol. 39, No. 1, 135–148, 2024.

[8] Dai, S., J. Wang, Z. Sun, and E. Chong, "Multiple current harmonics suppression for low-inductance PMSM drives with deadbeat predictive current control," *IEEE Transactions on Industrial Electronics*, Vol. 69, No. 10, 9817–9826, 2022.

[9] Bai, Y., B. Li, Q. Wang, D. Ding, G. Zhang, G. Wang, and D. Xu, "An adaptive-frequency harmonic suppression strategy based on vector reconstruction for current measurement error of PMSM drives," *IEEE Transactions on Power Electronics*, Vol. 38, No. 1, 34–40, 2023.

[10] Yang, J., J. Zhou, H. Zhou, F. Yi, D. Song, and M. Dong, "High-precision harmonic current extraction for PMSM based on multiple reference frames considering speed harmonics," *IEEE Transactions on Industrial Electronics*, Vol. 70, No. 10, 9764–9776, 2023.

[11] Zhang, Y., S. Li, B. Luo, C. Luo, and Z. Yu, "Output current harmonic analysis and suppression method for PMSM drive system with modular multilevel converter," *IET Renewable Power Generation*, Vol. 17, No. 13, 3289–3297, 2023.

[12] Chen, B., Z. Huang, P. Sun, and G. Wei, "Harmonic suppression for PMSM applied to MSTMP based on virtual even-order fractional repetitive controller," *IEEE Transactions on Industrial Informatics*, Vol. 20, No. 4, 6289–6299, Apr. 2024.

[13] Xie, F., J. Xu, M. Shen, and Z. Zheng, "Current harmonic suppression strategy for permanent magnet synchronous motor based on small phase angle resonant controller," *IET Electric Power Applications*, Vol. 18, No. 5, 556–564, 2024.

[14] Li, Y., Z. Yin, D. Yuan, Y. Zhang, Y. Gao, and H. Yang, "A Multi-Harmonics suppression backstepping extended state observer for the PMSM electrolytic capacitorless drives sensorless control," *IEEE Transactions on Power Electronics*, Vol. 40, No. 8, 10 769–10 782, 2025.

[15] Xu, J., Z. Wei, and S. Wang, "Active disturbance rejection repetitive control for current harmonic suppression of PMSM," *IEEE Transactions on Power Electronics*, Vol. 38, No. 11, 14 423–14 437, 2023.

[16] Ding, D., H. Xie, B. Li, G. Wang, R. Gao, Z. Ren, W. Yue, and D. Xu, "Harmonic suppression based on rectified current regulation with DC-link voltage decoupling for electrolytic capacitorless PMSM drives," *IEEE Transactions on Power Electronics*, Vol. 39, No. 2, 2213–2225, 2024.

[17] Zhang, Q., Y. Fan, J. Chen, C. Yang, and M. Cheng, "A current harmonic suppression method for PMSM based on harmonic prediction adaptive notch filter," *IEEE Transactions on Energy Conversion*, Vol. 37, No. 3, 2107–2118, 2022.